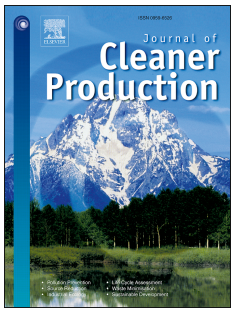

Microstructure and enhanced volume density properties of FeMn78C8.0 alloy prepared via a cleaner microwave sintering approach

Guo Chen, Kangqiang Li, Qi Jiang, Xinpei Li, Jinhui Peng, Mamdouh Omran, Jin Chen

PII: S0959-6526(20)31411-6

DOI: https://doi.org/10.1016/j.jclepro.2020.121364

Reference: JCLP 121364

To appear in: *Journal of Cleaner Production*

Received Date: 18 November 2019

Revised Date: 22 March 2020

Accepted Date: 25 March 2020

Please cite this article as: Chen G, Li K, Jiang Q, Li X, Peng J, Omran M, Chen J, Microstructure and enhanced volume density properties of FeMn78C8.0 alloy prepared via a cleaner microwave sintering approach, *Journal of Cleaner Production* (2020), doi: https://doi.org/10.1016/j.jclepro.2020.121364.

Author Contributions Section

Prof. Guo Chen, Prof. Jin Chen and Prof. Jinhui Peng conceived and designed the study. Mr. Kangqiang Li, Miss Qi Jiang, Dr. Mamdouh Omran and Prof. Guo Chen performed the experiments. Prof. Guo Chen and Prof. Jin Chen provided the raw materials. Prof. Jinhui Peng, Prof. Guo Chen and Mr. Xinpei Li provided the box-type microwave high temperature furnace. Mr. Kangqiang Li, Miss Qi Jiang and Prof. Jin Chen wrote the paper. Dr. Mamdouh Omran and Prof. Guo Chen reviewed and edited the manuscript. All authors read and approved the manuscript.

Microstructure and enhanced volume density properties of FeMn78C8.0 alloy prepared via a cleaner microwave sintering approach

Guo Chen [a, b], Kangqiang Li [a, b, **], Qi Jiang [b], Xinpei Li [b], Jinhui Peng [a, b], Mamdouh Omran [c], Jin Chen [a, b, *]

[a] *Key Laboratory of Green-Chemistry Materials in University of Yunnan Province, Kunming Key Laboratory of Energy Materials Chemistry, Yunnan Minzu University, Kunming 650500, P.R. China.*

[b] *Key Laboratory of Unconventional Metallurgy, Ministry of Education, Kunming University of Science and Technology, Kunming 650093, P.R. China.*

[c] *Process Metallurgy Research Group, Faculty of Technology, University of Oulu, Oulu 4600, Finland.*

* Corresponding author: jinchen@kust.edu.cn

** Co-corresponding author: guochen@kust.edu.cn

Abstract:

Smelting fine ore into a block with the lower phosphorus content before entering the furnace can achieve cleaner production and value-added efficiency for ferromanganese alloy enterprises, and microwave sintering technology shows bright application prospects in the secondary utilization of waste materials and environmental-friendly preparation of high-performance alloy materials. In this work, FeMn78C8.0 grade bulk alloy with enhanced volume density properties was efficiently prepared via an environmental-friendly microwave sintering approach, using high-carbon ferromanganese powder with low processing efficiency in factories as the raw material. Results indicate that adding certain carbon can prevent the oxidation behavior of Mn and Fe elements during the sintering process, and the qualified FeMn78C8.0 alloy can be obtained by controlling sintering temperature and duration time, with the optimum sintering conditions determined at 1168 °C for 11 min and with the alloy powder of <75 μm accounting for 63%. Meanwhile, some fine pores and cracks on the surface of FeMn78C8.0 alloy are conducive to the densification of the alloy sample and the internal alloying process of the carcass, further to enhance the volume density properties; and influence of the powder of <75 μm on the volume density properties is more profound than that by the powder of 75 μm-150 μm. Additionally, a higher value of volume density of 5.86 $g \cdot cm^{-3}$ is obtained at 1200 °C holding for 10 min, far beyond the traditionally produced alloy by electric furnace with an average value of 5.56 $g \cdot cm^{-3}$. The work highlights the efficient application of microwave sintering to the secondary utilization of ferromanganese powder and the environmental-friendly preparation of alloy materials.

Keywords: FeMn78C8.0 alloy; ferromanganese powder; microwave sintering; volume density; microstructure

1 Introduction

Ferromanganese is an alloy of manganese and iron made by smelting manganese ore, which has been widely used as deoxidizers, desulfurizers (Arcibar-Orozco et al., 2019) and alloying agents (Arshadi et al., 2019), to improve the ductility, hardness, anti-wear ability, and toughness properties of steel; in addition, its other applications have been extended to the fields of electronics (Kallitsis et al., 2020), catalysts (Cheng et al., 2020), agriculture, and national defense. Moreover, Adio et al. and Alswat et al. reported that ferromanganese-based magnetic materials can efficiently absorb lead, chromium, and thallium heavy metal ions from aqueous solutions (Adio et al., 2019; Alswat et al., 2016), and Tuzen et al. and Saleh et al. highlighted that ferromanganese-based magnetic materials can remove rhodamine and Bmethyl red hazards from waste water (Tuzen et al., 2018; Saleh and Al-Arfaj, 2017).

Ferromanganese is usually divided into three types identified by the carbon content: low-carbon ferromanganese (C%<0.7%), medium-carbon ferromanganese (C%=0.7%-2.0%), and high-carbon ferromanganese (C%=2.0%-8.0%) (Steenkamp et al., 2017). During the steelmaking process, high-carbon ferromanganese is the best additive when the molten steel needs to be added with both manganese (Mn) and carbon (C) (Zhang et al., 2009). However, about 10% of ferromanganese powder will be produced during the ferromanganese alloy production process; moreover, the market price of the powdered alloy is about 2000 RMB/ton lower than that of bulk alloy, attributed to the serious burning loss of powdered alloy when

added to molten steel (Zhang and Wu, 2004). Therefore, the efficient secondary utilization of ferromanganese powder to prepare bulk alloy implies unpredictable economic benefits for ferromanganese alloy enterprises. Currently, ferromanganese powder enterprises usually return these alloy powder into blast furnace or electric furnace for re-smelting, while this treatment changes the normal operation process of ferromanganese production, thus it comes with a poor economy and technicality (Zhang and Wu, 2004). Meanwhile, the large consume amount of coke and the introduced impurities in blast furnace method render it difficult to meet the quality requirements of manganese alloy for iron and steel industry (Zhang et al., 2009), and electric furnace method also has prominent shortcomings such as high energy consumption and low metal recovery rate (Tang et al., 2003). Therefore, there exists an urgent need to develop a new approach to process ferromanganese powder, which is cost effective and environmentally friendly to prepare the qualified bulk ferromanganese alloy materials.

As an environmental-friendly technology, microwave heating has gradually replaced the related applications of traditional heating in mineral pretreatment (Chen et al., 2020; Li et al., 2019a), medical sterilization, and chemical synthesis (Li et al., 2019b), etc. The essence of microwave heating is the process in which the heated material generates loss in its interior by the influence of the energy with high-frequency electromagnetic wave (Huang et al., 2020; Li et al., 2019c), followed by a thermal effect is formed, further to render the material to be heated (Zhou et al., 2019). Based on the unique heating characteristics, microwave heating has attracted increasing interest in powder processing (Li et al., 2020a), and gradually developed into a new technology for powder material sintering and alloy material preparation (Tao et al., 2020, Yao et al., 2020). Specifically, Vasudevan et al. reported a comparative

study of conventional and microwave sintering on the densification of TiC alloy, and highlighted that the sintering temperature was lowered to 1200 °C, and the density of the microwave sintered compact was 8%-10% higher than the conventionally sintered compact (Vasudevan et al., 2020). Cai et al. utilized microwave sintering to replace traditional sintering to successfully fabricate $Bi_{0.9}La_{0.1}FeO_3$ ceramics, and reported that the microwave sintered BLF ceramics possessed a higher densification and enhanced ferroelectric and magnetic properties, and the leakage current can be significantly decreased (Cai et al., 2019). Deng et al. synthesized Ce/Mn dual-doped $LaAlO_3$ ceramics with enhanced far-infrared emission capability via microwave sintering approach, and results indicated Ce/Mn co-doping caused the enhancement of lattice strain and asymmetrical vibration, and verified that microwave sintering is a high-efficiency method for perovskite-type phase formation (Deng et al., 2019). In summary, microwave sintering technology can greatly shorten the sintering temperature and processing time, achieving the environment-friendly and energy efficient preparation of alloy materials. Moreover, when the particle size of the metal is decreased to micron or even nanometer grade, the microwave heating characteristics will change (Allamia et al., 2019; Li et al., 2020b). The penetration depth of microwave in bulk metal is very small, but in metal powder, the penetration depth is equivalent as the powder with a particle size at the same order of magnitude (Liu et al., 2018). When microwave energy heats the metal powder, the volume of the part coupled with microwave accounts for a large part of the total volume (Li et al., 2020c; Mane et al., 2020). In addition, there exist a large number of voids in the metal powder, and through these voids, the required microwave energy can directly enter the interior of the powder (Li et al., 2020d); meanwhile, the reflected microwave energy by

the metal particles is effectively limited to the interior of the powder and will be absorbed by other metal particles, further rendering microwave heating can significantly increase the temperature of metal powder (Li et al., 2020e). Therefore, based on the high microwave absorption characteristics of some alloy powder, it can be speculated that the bulk alloy can be rapidly prepared from ferromanganese powder through microwave sintering, which will bring potential and considerable economic benefits to ferromanganese alloy production enterprises.

Tricky problems exist in the treatment of ferromanganese powder by traditional blast furnace and electric furnace methods, like high energy consumption, low metal recovery rate, and low product performance, severely restricting the continuous production and clean production of industry. Meanwhile, the superiority of the efficient applications of microwave heating replacing traditional heating to the secondary utilization of waste materials and cleaner production of high-performance alloy materials has been frequently highlighted. However, there is absent of a detailed work regarding the combination of the cleaner preparation of bulk alloy and the secondary utilization of ferromanganese powder by microwave sintering. Hence, in the present work, the merits of the novel method for ferromanganese powder sintering were attempted to assess, using microwaves as the energy source. Detailedly, effects of sintering process parameters on the volume density properties and microstructure of the sintered bulk alloy were comparatively determined to clarify the ferromanganese powder sintering process, including sintering temperature, duration time, and composition proportion of ferromanganese powder with different sizes, further to explore the

scientific feasibility and effectiveness of microwave sintering on the cleaner preparation of bulk alloy and the secondary utilization of ferromanganese powder.

2 Experimental

Ferromanganese powder as the research object was expected to be sintered into bulk alloy by microwave sintering approach, to achieve the cleaner preparation of bulk alloy and the secondary utilization of ferromanganese powder. The detailed information about the ferromanganese powder material, characterization methods, microwave sintering furnace, and experimental procedure was detailed as follows.

2.1 Materials

Ferromanganese powder was used as the raw material, received from Wenshan city (Yunnan Province, P.R. China). The chemical compositions of ferromanganese powder were illustrated in Table 1, as follows: Mn, 76.47%; Fe, 15.53%; C, 6.40%; Si, 1.41%; P, 0.17%; S, 0.02%, respectively. The analytical results were performed by the National Standard method of the People's Republic of China (GB/T3975-2006). Concluded from Table 1, the ferromanganese powder was characterized by high carbon content (2.0%-8.0%) and high phosphorus content (0.17%). In the iron and steel industry, the low content of phosphorus in ferromanganese alloy additive can significantly enhance the quality of steel (Guo et al., 1998; Lai et al., 2016). Therefore, if the high-carbon ferromanganese powder could be sintered into a bulk alloy and meanwhile the phosphorus (P) content could be decreased, the economic benefits to enterprises will be incalculable, meanwhile achieving energy-saving emission reduction and value-added efficiency for ferromanganese alloy enterprises.

The particle size distribution of the ferromanganese powder was depicted in Fig. 1. As depicted in Fig. 1, the ferromanganese powder was characterized with the median particle diameter (D_{50}) of 156.15 μm, and the particle size of the measured powder was basically less than 250 μm. Wherein the particle size of >150 μm accounted for 47.8% (mass percentage), the particle size of 75 μm-150 μm accounted for 47.1% (mass percentage), and the proportion of the particle size of <75 μm accounted for 5.1% (mass percentage).

2.2 Characterization

The microstructure appearance of the ferromanganese powder and the sintered alloy samples were analyzed by a scanning electron microscope (Phenom ProX, Phenom-World, Netherlands), and the attached energy dispersion scanner spectrometer (EDAX, Phenom-World, Netherlands) was utilized to determine the semi-quantitative chemical analysis for the sintered alloy samples. The simultaneous thermal analyzer (STA 449F3, NETZSCH, Germany) was applied to determine the thermo-gravimetric analysis for the ferromanganese powder, measured at a temperature regime of 20 °C to 1350 °C, with 30 °C/min of the heating rate, and with Argon (Ar) as the shielding gas at a flow rate of 60 mL/min and taking Al_2O_3 as the reference material.

2.3 Instrumentation

Microwave vacuum sintering furnace (MAKEWAVE) was applied to conduct the sintering experiments for ferromanganese powder. The microwave furnace was mainly composed by microwave reactor, vacuum pump, infrared thermocouple, rotation, motor, insulating brick, flowmeter, gas generator, and a computer control system. Based on the different experimental demands, the protective gas can be chosen to be injected into the

microwave reactor cavity, and the microwave power was supplied by two magnetrons at 2450 MHz microwave frequency, with a continuous controllable regime of 0-3 kW. The attached infrared thermocouple (Marathon Series, Raytek, USA) measured the instant temperature of the sample, accompanying with a service temperature ranging from 450 °C to 1600 °C. The microwave furnace was equipped with two operating modes, with manual mode and automatic mode for switching. By the way, the operating mode was selected with automatic mode during the sintering experiments for ferromanganese powder.

2.4 Procedure

The process flow chart of preparing bulk alloy by microwave sintering was illustrated in Fig. 2. Firstly, the high-carbon ferromanganese powder was dried by an electric blast drying oven (DHG9079A) at 105 °C for 12 h, aiming to remove the moisture in the powder. Then, the dried powder was milled and screened to be divided into three powders identified by the following particle size range: <75 μm, 75 μm-150 μm, >150 μm. Meanwhile, the two powders with the respective particle size of <75 μm and 75 μm-150 μm were selected out to be mixed in a porcelain mortar for 10 min, with different mixing proportions varying from 0%, 25%, 50%, 75%, and 100%. The mass of each mixed sample was constant at 100.0 g, followed by the mixed samples were introduced into a ceramic crucible and placed in the center of the microwave furnace, with the box body sealed. Next, Argon (Ar) was injected in the microwave furnace for vacuuming, with lasting for 10 min and a flow rate of 150 sccm. After vacuuming, the sintering temperature and duration time were set, with the microwave furnace operating in automatic mode. Wherein the sintering temperatures were controlled to vary from 1000 °C, 1050 °C, 1100 °C, 1150 °C, and 1200 °C, and the duration times were

controlled to vary from 0 min to 20 min, with 5 min as a variable node. Once reaching the expected sintering temperature and duration time, the sintered samples were removed and cooled with the microwave furnace to room temperature by oxygen insulation, followed by the volume density properties and the chemical compositions of the sintered samples were determined.

After the sintering experiments, every sintered bulk alloy sample was subjected to wire electric discharge cutting and processed into three standard samples, all having a size of 10 mm×10 mm×10 mm, and the masses of the standard samples were weighed by an electronic balance (Tricle-QD-1). After measuring the volume density of the cut three standard samples, the volume density of the sintered bulk alloy was determined by taking the average value among the three values, and with the error analysis conducted. The volume density properties of bulk alloy are determined by the following Eq. (1),

$$\rho = \frac{m}{V} \tag{1}$$

Where ρ means the volume density of the standard sample; m indicates the mass of the standard sample; V denotes the volume of the standard sample (10 mm ×10 mm ×10 mm).

3 Results and discussion

Thermodynamics analysis and thermo-gravimetric analysis can determine the thermal behavior of the ferromanganese powder; additionally, volume density properties analysis was conducted to explore the effects of sintering factors on the volume density properties, and microstructure and composition characterization can investigate the change in microstructure micromorphology of the ferromanganese powder during microwave sintering process. All

those analysis can contribute to clarify the sintering process of ferromanganese powder by microwave sintering.

3.1 Thermodynamics analysis

Thermodynamics analysis can explore the chemical reactions in the ferromanganese powder, further contributing to clarify the sintering process of ferromanganese powder by microwave sintering. According to the chemical compositions of high-carbon ferromanganese powder (Table 1), the main elements in the powder sample were Mn, Fe, C, and Si, with a small content of P and S. Therefore, to simplify the thermodynamic calculation, the influence of P and S elements can be omitted. The thermodynamics data of the oxidation reactions of elements in alloy melt were calculated by thermodynamic software including Fact-sage and HSC 6.0, presented in Table 2, wherein ΔH^{θ} indicates the enthalpy change of reaction, and ΔS^{θ} means the entropy change of reaction. The two definitions are both functions of temperature, and their changes with temperature are similar in many reactions. Therefore, those changes can cancel each other, rendering a small nonlinearity of ΔG^{θ} with temperature.

The dependency of ΔG^{θ} on temperatures for oxidation reactions of elements in alloy melt was illustrated in Fig. 3. As depicted in Fig. 3, the ΔG^{θ} negative value of the reactions between Mn, Fe, Si and other elements with oxygen (O_2) presented a decreasing trend with temperature improving, while the ΔG^{θ} negative value of the reaction between carbon (C) element and oxygen (O_2) presented an increasing trend with temperature improving. From the intersections of the line of the oxidation reaction of carbon (C) and the line of the oxidation reactions of other elements, it can be concluded that carbon (C) could reduce FeO at temperatures higher than 660 °C; and when temperatures exceeded 1392 °C, carbon (C) can

reduce MnO; at temperatures above 1773 °C, carbon (C) can reduce all oxides. In the iron and steel industry, the low content of phosphorus in ferromanganese alloy additive can significantly enhance the quality of steel (Guo et al., 1998), and the content of iron (Fe) and manganese (Mn) should maintain the original level as much as possible to ensure the grade of ferromanganese alloy (Lai et al., 2016). Therefore, the sintering temperature was considered to be controlled at 660 °C-1392 °C, aiming to prevent the oxidations of Fe and Mn element and meanwhile to avoid or decrease the influence of other impurity elements like P and S elements, further to obtain the expected qualified ferromanganese alloy.

3.2 Thermo-gravimetric analysis

Thermo-gravimetric analysis can determine the thermal behavior of the ferromanganese powder, further contributing to clarify the sintering process of ferromanganese powder by microwave sintering. The melting point of high-carbon ferromanganese alloy is related to its chemical compositions (Saleh, 2018). During the heating process, physical and chemical changes will occur, such as drying, crystal transformation, melting, decomposition, and oxidation reactions, accompanying with endothermic and exothermic phenomena (Saleh, 2016). The thermo-gravimetric measurement was conducted to roughly determine the burning loss behavior and the melting point of ferromanganese powder, and the TG-DSC curves were plotted in Fig. 4.

As depicted in Fig. 4, it can be observed from the TG curve that there were three obvious weightlessness processes during the heating process of ferromanganese powder. At the temperature section between 20 °C and 200 °C, the weight change was mainly attributed to the oxidization reactions of alloy elements (Adio et al., 2017). Based on Table 2 and Fig. 3, it

can be concluded that the oxidization reactions of Mn and Fe elements can spontaneously proceed, wherein Mn and Fe elements were oxidized into the corresponded metal oxides, and followed by metal oxides were converted into metal carbides, which is attributed to the affinity of carbon (C) with metal is higher than that of oxygen (O) (Saleh and Naeemullah, 2017). Therefore, the new generated metal oxides metal carbides of Mn and Fe elements rendered the increment of weight at this temperature regime. For the temperature section between 200 °C and 660 °C, the weight loss was mainly ascribed to the oxidization reaction of $2C(S) + O_2(g) = 2CO(g)$, wherein carbon (C) was oxidized into carbon monoxide (CO), escaping as the gas, further rendering the weight loss at this temperature regime. Additionally, at the temperature section between 660 °C and 1240 °C, the weight loss was assigned to that carbon (C) inhibited the oxidization reaction of $2Fe(l) + O_2(g) = 2FeO(s)$, causing the metal oxides FeO produced at the early stage was reduced into Fe element (Saleh., 2018), further to cause the weight loss at this temperature regime. Moreover, at temperatures exceeding 1240 °C, the sample showed little mass change. The total weight loss rate was 9.08%. The TG-DSC curves are affected by many factors, such as sample quantity, heating rate, gas, etc. Therefore, the melting temperature measured had certain reference value and deviated from the actual melting point. From the DSC curve, it was observed that point A corresponded to an endothermic peak, with a temperature of 1200 °C, which was exactly the melting point of the crystal melt.

3.3 Volume density properties analysis

The density properties of ferromanganese alloy when encountered an external force are usually evaluated by volume density, which are influenced by composition, particle size,

duration time, and sintering temperature (Alade et., 2019; Saleh., 2014). Therefore, in this work, effects of sintering factors on the volume density properties of the sintered alloy were investigated, including temperature, duration time and composition proportion of alloy powder with different particle sizes. The obtained results were depicted in Fig. 5.

Fig. 5(a) illustrated the effects of sintering temperature on the volume density properties of the sintered bulk alloy, controlling temperature varied from 1000 °C, 1050 °C, 1100 °C, 1150 °C and 1200 °C, under the constant conditions with the composition content of particle size of <75 μm accounting 75% and duration time of 10 min. As observed from Fig. 5(a), the volume density properties of the sintered bulk alloy increased with sintering temperature, having a volume density of only 4.72 $g \cdot cm^{-3}$ at 1100 °C; while it suddenly jumped to 5.69 $g \cdot cm^{-3}$ at temperature of 1150 °C and 5.86 $g \cdot cm^{-3}$ at 1200 °C, respectively, which the values were far higher than that of the original ferromanganese alloy produced by commercial ferromanganese alloy enterprises, with an average value of 5.56 $g \cdot cm^{-3}$. The changing trend of volume density properties indicated that increasing sintering temperature contributed to improving the volume density properties of ferromanganese alloy. Increasing sintering temperature is beneficial to the densification of the sample (Hou et al., 2019), promoting the internal alloying process of the carcass (Ye et al., 2018), further to render the volume density properties enhanced.

Fig. 5(b) presented the effects of duration time on the volume density properties of the sintered bulk alloy, controlling duration time varied from 0 min to 20 min, under the constant conditions with the composition content of particle size of <75 μm accounting 75% and the sintering temperature of 1100 °C. As presented in Fig. 5(b), the volume density of the sintered

bulk alloy was determined with an initial value of 4.47 $g \cdot cm^{-3}$, which was much lower than that of the original ferromanganese alloy produced by commercial ferromanganese alloy enterprises; while it suddenly improved to a maximum of 4.98 $g \cdot cm^{-3}$ within a duration of 15 min. This phenomenon indicated that extending the duration time can increase the degree of densification of the carcass, thereby enhancing the volume density properties of the sintered bulk alloy. While duration time exceeded 15 min, the volume density was observed to present a decreasing trend with duration time increasing, which was attributed to the fact that prolonging the duration time can provide more time for the gas discharge inside the carcass (Hou et al., 2019), wherein the gas was produced from the oxidization reactions of carbon (C), phosphorus (P), and sulfur (S); meanwhile, the powder particles inside the carcass were rearranged and the diffusion of the liquid phase was more fully (Ye et al., 2018). However, under such high-temperature conditions at 1100 °C, too long duration time will cause the loss of liquid phase, further to increase the abnormal growth of the first-order crystal grains (Hou et al., 2019; Ye et al., 2018), rendering the volume density properties of the sintered bulk alloy decreased.

From Fig. 1, it can be observed that the proportion of the ferromanganese powder of <75 μm accounted for less than 7%, and the ferromanganese powder of >150 μm accounted for 47%. Considering that the ferromanganese powder with particle size of 75 μm-150 μm presented better heating characteristics than that of the powder of <75 μm in microwave field (Li and Zhang, 2018; Saleh., 2015a), hence using the powder of <75 μm to prepare bulk alloy by microwave sintering will undoubtedly increase the difficulty and energy consumption of sintering process. Therefore, in the present work, the powder of <75 μm and the powder of 75

μm-150 μm were selected out to mixed, and the mixed samples were sintered , further to explore effects of the composition proportion of the alloy powder of <75 mm on the volume density properties of the sintered bulk alloy. The obtained results were plotted in Fig. 5(c), controlling the mixing proportion covering 0%, 25%, 50%, 75%, and 100%, under the constant conditions with the sintering temperature of 1100 °C and the duration time of 10 min. As observed from Fig. 5(c), the value of the volume density of the sintered bulk alloy increased initially, followed by it decreased with the composition proportion of the powder of <75 mm improving. Meanwhile, as illustrated in Fig. 5(c), the slope of the rising curve increased gradually until the content improved to 50%, then decreased slightly. When the ferromanganese powder of 75 μm-150 μm accounted for 100%, the value of the volume density of the sintered bulk alloy was only 4.36 $g \cdot cm^{-3}$, which was significantly lower than that of the sintered bulk alloy prepared with all the alloy powder of <75 μm, having a value of 4.70 $g \cdot cm^{-3}$. When the composition proportion of the alloy powder of <75 mm was 50%, the volume density of sintered samples increased to 4.75$g \cdot cm^{-3}$. From the above analysis, it could be concluded that mixing alloy powder of different particle sizes was beneficial to improve the volume density properties of the sintered bulk alloy, and an increase in the composition proportion of the alloy powder of <75 mm had a more profound effect than the alloy powder of 75 μm-150 μm.

Combined with Fig 5(a) and Fig 5(b), it was summarized that all values of the volume density of the bulk alloys sintered at 1100 °C were much lower than that of the original ferromanganese alloy produced by commercial ferromanganese alloy enterprises, with an average value of 5.56 $g \cdot cm^{-3}$. While under the duration of 10 min, the volume density jumped

from 4.72 g·cm^{-3} at 1100 °C to 5.69 g·cm^{-3} at 1150 °C, which the value at 1150 °C was higher than that of the original alloy; with temperatures higher than 1150 °C, the increment in volume density became slight. Therefore, it could be speculated that the optimum microwave sintering temperature may be close to 1150 °C. Through the above analysis, it was found that the ferromanganese powder can be quickly sintered into a bulk alloy by microwave sintering, at a lower temperature than the melting point of ferromanganese powder (1220 °C-1270 °C) (Saleh., 2015b), denoting microwave sintering reduced the sintering temperature of ferromanganese alloy prepared by traditional sintering methods. Moreover, under suitable process conditions, the volume density properties of the bulk alloy prepared by microwave sintering were comparable to that of the original alloy.

3.4 Microstructure and composition characterization

After crushing the bulk alloy sintered under different conditions, representative alloy blocks were selected for grinding and polishing to observe and compare the change of surface micromorphology, the obtained SEM images and EDAX spectra were presented in Fig.6 and Fig. 7.

Fig. 6(a) presented the microstructure micromorphology of the ferromanganese powder. As seen from Fig. 6(a), the powder particles presented no fixed shape, being angular with a thick middle and thin edge, meanwhile, a large number of fine particles existed. Fig. 6(b) displayed the SEM image of the bulk alloy obtained under the optimal process conditions, with the sintering temperature of 1168 °C and the duration time of 11 min and the alloy powder of <75 μm accounting for 63%, wherein the optimum sintering conditions were optimized by response surface method. As displayed in Fig. 6(b), the morphology of the

sintered bulk alloy was completely different from that of ferromanganese powder, which was similar to that of the whole alloy, but a very small number of fine pores and cracks appeared on the surface, which are conducive to the densification of the alloy sample and the internal alloying process of the carcass, further to enhance the volume density properties of the sintered bulk alloy. The microstructure change was attributed to that microwave heating endows the unique selective heating characteristics. Ferromanganese alloy elements endow excellent microwave-absorbing properties, like Mn and Fe elements (Li et al., 2019c); therefore, these alloy elements can be heated to a higher temperature during the same treatment process. While the weak microwave-absorbing materials were difficult to heat, like gangue (SiO_2) (Huang et al., 2020), therefore a large temperature gradient is formed between the alloy elements and gangue components, further to render the formation of thermal stress at the interface and the structural cracks (Zhou et al., 2019).

Fig. 7 illustrated the SEM images and EDAX spectra of the bulk alloy sintered at 1168 °C for 11 min. From the EDAX spectra, it was determined that the main elemental compositions of the sintered bulk alloy contained Mn and Fe elements, with a small amount of C element, without phosphorus (P) determined. In the iron and steel industry, the low content of phosphorus in ferromanganese alloy additive can significantly enhance the quality of steel grades (Guo et al., 1998; Lai et al., 2016). And the characteristics of oxidative dephosphorization of ferromanganese are different from the dephosphorization in molten iron: on the one hand, the difficulty of ferromanganese dephosphorization is large, and the CaO-based slag system commonly used in iron and steel smelting is difficult to meet the requirements, hence a BaO-based slag system with stronger dephosphorization capacity is

required. On the other hand, ferromanganese dephosphorization must be performed under the premise of preventing oxidation loss of manganese (Guo et al., 1998; Lai et al., 2016). Therefore, to evaluate the superiority of microwave sintering approach to prepare ferromanganese alloy, the change in phosphorus content of ferromanganese alloy during microwave sintering process needed to be discerned more clearly. Table 3 presented the chemical compositions of the bulk alloy sintered at 1168 °C for 11 min. It can be summarized from Table 3 that the manganese content was absent of oxidation loss, the sintered bulk alloy met the chemical composition standard of FeMn78C8.0 grade. Meanwhile, the average volume density of the bulk alloy sintered obtained at the optimum conditions was 5.71 $g \cdot cm^{-3}$, which also exceeded the requirements during factory production. Moreover, the decrease of phosphorus content in bulk alloy is beneficial to improve the temper brittleness, hot workability and weldability of steel in subsequent production (Guo et al., 1998; Lai et al., 2016). Combined with Table 1 and Table 3, it can be summarized that after microwave sintering treatment, the phosphorus content of the bulk alloy was 0.12%, much lower than that of the original ferromanganese powder (0.17%). The decrease of phosphorus content was attributed to the phosphorus element was oxidized into the corresponded oxides, escaping as the form of gas. From the above analysis, the qualified FeMn78C8.0 grade alloy with the lower phosphorus content was efficiently prepared by microwave sintering method, using the waste ferromanganese powder as the raw material, achieving the combination of the cleaner preparation of bulk alloy and the secondary utilization of ferromanganese powder.

4 Conclusions

In this work, a novel cleaner method for preparing FeMn78C8.0 bulk alloy was proposed, using ferromanganese powder as the raw material and microwave sintering to replace traditional sintering methods. Results indicated that adding certain amount of carbon can prevent the oxidation loss of Mn and Fe. The optimum sintering conditions were determined at 1168 °C for 11 min and with the alloy powder of <75 μm accounting for 63%. The powder of <75 μm presented a significantly better effect than the powder of 75 μm-150 μm for enhancing the volume density properties. The microwave sintered bulk alloy possessed an enhanced volume density of 5.86 $g \cdot cm^{-3}$, meanwhile with the much lower phosphorus content, far better than that of the ferromanganese alloy traditionally produced. Moreover, fine pores and cracks appeared on the morphology of the bulk alloy, which was attributed to the unique selective heating characteristics of microwave heating. The work confirms the cleaner preparation of FeMn78C8.0 bulk alloy by microwave sintering, with enhanced volume density properties and the lower phosphorus content; furthermore, the work can provide some sound reference for applying microwave sintering to the combination of the environmental-friendly preparation of alloy materials and the secondary utilization of powder materials.

Acknowledgments

Financial supports from the National Natural Science Foundation of China (No: U1802255) and Innovative Research Team (in Science and Technology) in University of Yunnan Province were sincerely acknowledged.

References

Adio, S.O., Asif, M., Mohammed, A.I., Baig, N., Al-Arfaj, A.A., Saleh, T.A., 2019. Poly (amidoxime) modified magnetic activated carbon for chromium and thallium adsorption: Statistical analysis and regeneration. Process. Saf. Environ. 121, 254-262. https://doi.org/10.1016/j.psep.2018.10.008.

Adio, S.O., Omar, M.H., Asif, M., Saleh, T.A., 2017. Arsenic and selenium removal from water using biosynthesized nanoscale zero-valent iron: A factorial design analysis. Process. Saf. Environ. 107, 518-527. https://doi.org/10.1016/j.psep.2017.03.004.

Alade, I.O., Rahman, M.A.A., Saleh, T.A., 2019. Modeling and prediction of the specific heat capacity of Al_2O_3/water nanofluids using hybrid genetic algorithm/support vector regression model. Nano-Structures. Nano-Objects. 17, 103-111. https://doi.org/10.1016/j.nanoso.2018.12.001.

Allamia, A.H., Tabasizadeha, M., Rohania, A., Farzada, A., Nayebzadehb, H., 2019. Precise evaluation the effect of microwave irradiation on the properties of palm kernel oil biodiesel used in a diesel engine. J. Clean. Prod. 241, 117777. https://doi.org/10.1016/j.jclepro.2019.117777.

Alswat, A.A., Ahmad, M.B., Saleh, T.A., 2016. Zeolite modified with copper oxide and iron oxide for lead and arsenic adsorption from aqueous solutions. J. Water. Supply. Res. T. 65(6), 465-479. https://doi.org/10.2166/aqua.2016.014.

Arcibar-Orozco, J.A., Acosta-Herrera, A.A., Rangel-Mendez, J.R., 2019. Simultaneous desulfuration and denitrogenation of model diesel fuel by Fe-Mn microwave modified

activated carbon: Iron crystalline habit influence on adsorption capacity. J. Clean. Prod. 218, 69-82. https://doi.org/10.1016/j.jclepro.2019.01.202.

Arshadi, M., Yaghmaei, S., Mousavi, S.M., 2019. Optimal electronic waste combination for maximal recovery of Cu-Ni-Fe by Acidithiobacillus ferrooxidans. J. Clean. Prod. 240, 118077. https://doi.org/10.1016/j.jclepro.2019.118077.

Cai, W., Gao, R.L., Fu, C.L., Yao, L.W., Chen, G., Deng, X.L., Wang, Z.H., Cao, X.L., Wang, F.Q., 2019. Microstructure, enhanced electric and magnetic properties of $Bi_{0.9}La_{0.1}FeO_3$ ceramics prepared by microwave sintering. J. Alloy. Compd. 774, 61-68. https://doi.org/10.1016/j.jallcom.2018.09.316.

Chen, G., Jiang, Q., Li, K.Q., He, A.X., Peng, J.H., Omran, M., Chen, J., 2020. Simultaneous removal of Cr(III) and V(V) and enhanced synthesis of high-grade rutile TiO_2 based on sodium carbonate decomposition. J. Hazard. Mater. 388, 122039. https://doi.org/10.1016/j.jhazmat.2020.122039.

Cheng, Y., Zhang, S.S., Huang, T.L., Cheng, L.J., Yao, X., 2020. Effects of coagulants on the catalytic properties of iron-manganese co-oxide filter films for ammonium and manganese removal from surface water. J. Clean. Prod. 242, 118494. https://doi.org/10.1016/j.jclepro.2019.118494.

Deng, Y., Zhang, K.W., Yang, Y.Y., Shi, X.Y., Yang, L., Yang, W.Z., Wang, Y., Chen, Z.G., 2019. Ce/Mn dual-doped $LaAlO_3$ ceramics with enhanced far-infrared emission capability synthesized via a environmental-friendly microwave sintering method. Ceram. Int. 774, 434-442. https://doi.org/10.1016/j.jallcom.2018.10.049.

Guo, S.X., Dong, Y., 1998. Experimental study on dephosphorization of ferromanganese alloys by BaO-halide fluxes. Iron. Steel. 33(1), 26-28. https://doi.org/10.3321/j.issn:0449-749X.1998.01.006.

Huang, L., Ding, S.H., Yan, X.K., Song, T.X., Zhang, Y., 2020. Structure and microwave dielectric properties of $BaAl_2Si_2O_8$ ceramic with Li_2O-B_2O_3 sintering additive. J. Alloy. Compd. 820, 153100. https://doi.org/10.1016/j.jallcom.2019.153100.

Hou, M., Guo, S.H., Yang, L., Ullah, E., Gao, J.Y., Hu, T., Ye, X.L., Hu, L.T., 2019. Microwave hot press sintering: New attempt for the fabrication of Fe-Cu pre-alloyed matrix in super-hard material. Powder. Technol. 356, 403-413. https://doi.org/10.1016/j.powtec.2019.08.055.

Kallitsis, E., Korre, A., Kelsall, G., Kupfersberger, M., Nie, Z.G., 2020. Environmental life cycle assessment of the production in China of lithium-ion batteries with nickel-cobalt-manganese cathodes utilising novel electrode chemistries. J. Clean. Prod. 254, 120067. https://doi.org/10.1016/j.jclepro.2020.120067.

Lai, C.B., Xi, X.J., Gan, L., Peng, Y.L., Zhang, Z.M., Liu, T.G., 2016. Review on dephosphorization for ferromanganese alloy. Nonferr. Met. Sci. Eng. 7(2), 32-38. https://doi.org/10.13264/j.cnki.ysjskx.2016.02.006.

Li, K.Q., Chen, J., Chen, G., Peng,, J.H., Ruan, R., Srinivasakannan, C., 2019a. Microwave dielectric properties and thermochemical characteristics of the mixtures of walnut shell and manganese ore. Bioresource. Technol. 286, 121381. https://doi.org/10.1016/j.biortech.2019.121381.

Li, K.Q., Chen, G., Chen, J., Peng, J.H., Ruan, R., Srinivasakannan, C., 2019b. Microwave pyrolysis of walnut shell for reduction process of low-grade pyrolusite. Bioresource. Technol. 291, 121838. https://doi.org/10.1016/j.biortech.2019.121838.

Li, K.Q., Chen, G., Li, X.T., Peng, J.H., Ruan, R., Omran, M., Chen, J., 2019c. High-temperature dielectric properties and pyrolysis reduction characteristics of different biomass-pyrolusite mixtures in microwave field. Bioresource. Technol. 294, 122217. https://doi.org/10.1016/j.biortech.2019.122217.

Li, K.Q., Chen, J., Peng, J.H., Ruan, R., Srinivasakannan, C., Chen, G., 2020a. Pilot-scale study on enhanced carbothermal reduction of low-grade pyrolusite using microwave heating. Powder. Technol. 360, 846-854. https://doi.org/10.1016/j.powtec.2019.11.015.

Li, K.Q., Chen, J., Peng, J.H., Koppala, S., Omran, M., Chen, G., 2020b. One-step preparation of CaO-doped partially stabilized zirconia from fused zirconia. Ceram. Int. 46(5), 6484-6490. https://doi.org/10.1016/j.ceramint.2019.11.129.

Li, K.Q., Jiang, Q., Chen, J., Peng, J.H., Li, X.P., Koppala, S., Omran, M., Chen, G., 2020c. The controlled preparation and stability mechanism of partially stabilized zirconia by microwave intensification. Ceram. Int. In press. https://doi.org/10.1016/j.ceramint.2019.11.251.

Li, K.Q., Chen, J., Peng, J.H., Ruan, R., Orman, M., Chen, G., 2020d. Dielectric properties and thermal behavior of electrolytic manganese anode mud in microwave field. J. Hazard. Mater. 381, 121227. https://doi.org/10.1016/j.jhazmat.2019.121227.

Li, K.Q., Chen, J., Peng, J.H., Orman, M., Chen, G., 2020d. Efficient improvement for dissociation behavior and thermal decomposition of manganese ore by microwave

calcination. J. Clean. Prod. In press, 121074. https://doi.org/10.1016/j.jclepro.2020.121074.

Li, L., Zhang, L.B., Dai, L.Q., Zhu, H.B., Chen, G., Peng, J.H., Guo, Q., 2018. Effects of microwave sintering of properties and microstructure of ferromanganese alloy powders. Arch. Metall. Mater. 63(2), 547-553. https://doi.org/10.24425/118973.

Liu, C., Peng, J.H., Zhang, L.B., Wang, S.X., Ju, S.H., Liu, C.H., 2018. Mercury adsorption from aqueous solution by regenerated activated carbon produced from depleted mercury-containing catalyst by microwave-assisted decontamination. J. Clean. Prod. 196, 109-121. https://doi.org/10.1016/j.jclepro.2018.06.027.

Mane, S.M., Pawar, S.A., Patil, D.S., Kulkarni, S.B., Tayade, N.T., Shin, J.C., 2020. Magnetoelectric, magnetodielectric effect and dielectric, magnetic properties of microwave-sintered lead-free $x(Co_{0.9}Ni_{0.1}Fe_2O_4)$-$(1-x)[0.5(Ba_{0.7}Ca_{0.3}TiO_3)$-$0.5(BaZr_{0.2}Ti_{0.8}O_3)]$ particulate multiferroic composite. Ceram. Int. 46(3), 3311-3323. https://doi.org/10.1016/j.ceramint.2019.10.038.

Saleh, T.A., 2014. Spectroscopy: between modeling, simulation and practical investigation. Spectral Analysis Review. 2(01), 1-2. https://doi.org/10.4236/sar.2014.21001.

Saleh, T.A., 2015a. Mercury sorption by silica/carbon nanotubes and silica/activated carbon: a comparison study. J. Water. Supply. Res. T. 64(8), 892-903. https://doi.org/10.2166/aqua.2015.050.

Saleh, T.A., 2015b. Isotherm, kinetic, and thermodynamic studies on Hg(II) adsorption from aqueous solution by silica- multiwall carbon nanotubes. Environ. Sci. Pollut. R. 22(21), 16721-16731. https://doi.org/10.1007/s11356-015-4866-z.

Saleh, T.A., 2016. Nanocomposite of carbon nanotubes/silica nanoparticles and their use for adsorption of Pb(II): from surface properties to sorption mechanism. Desalin. Water. Treat. 57 (23), 10730-10744. https://doi.org/10.1080/19443994.2015.1036784.

Saleh, T.A., 2018. Simultaneous adsorptive desulfurization of diesel fuel over bimetallic nanoparticles loaded on activated carbon. J. Clean. Prod. 172, 2123-2132. https://doi.org/10.1016/j.jclepro.2017.11.208.

Saleh, T.A., Al-Arfaj, A.A., 2017. Kinetics, isotherms and thermodynamic evaluation of amine functionalized magnetic carbon for methyl red removal from aqueous solutions. J. Mol. Liq. 248, 577-585. https://doi.org/10.1016/j.molliq.2017.10.064.

Saleh, T.A., Naeemullah, Tuzen, M., Sarı, A., 2017. Polyethylenimine modified activated carbon as novel magnetic adsorbent for the removal of uranium from aqueous solution. Chem. Eng. Res. Des. 117, 218-227. https://doi.org/10.1016/j.cherd.2016.10.030.

Saleh, T.A., Tuzen, M., Sarı, A., 2018. Polyamide magnetic palygorskite for the simultaneous removal of Hg(II) and methyl mercury; with factorial design analysis. J. Environ. Manage. 211, 323-333. https://doi.org/10.1016/j.jenvman.2018.01.050.

Steenkamp, J.D., Hockaday, C.J., Gous, J.P., Nzima, T.W., 2017. Dissipation of electrical energy in submerged arc furnaces producing silicomanganese and high-carbon ferromanganese. JOM. 69(9), 1712-1716. https://doi.org/10.1007/s11837-017-2434-3.

Tang, F.C., Yan, K.S., Chen, J.W., 2003. Brief analysis of the gas purification and comprehensive utilization for Mn-Si furnace. Ferro-Alloys. 34, 38-43. https://doi.org/ 10.3969/j.issn.1001-1943.2003.03.011.

Tuzen, M., Sarı, A., Saleh, T.A., 2018. Response surface optimization, kinetic and thermodynamic studies for effective removal of rhodamine B by magnetic AC/CeO_2 nanocomposite. J. Environ. Manage. 206, 170-177. https://doi.org/10.1016/j.jenvman.2017.10.016.

Vasudevan, N., Nasir Ahamed, N. N., B, P., Aravindhan, A., Shanmugavel, B. P., 2020. Effect of Ni addition on the densification of TiC: A comparative study of conventional and microwave sintering. Int. J. Refract. Met. H. 87, 105165. https://doi.org/10.1016/j.ijrmhm.2019.105165.

Tao, S.C., Xu, J.L., Yuan, L., Luo, J.M., Zheng, Y.F., 2020. Microstructure, mechanical properties and antibacterial properties of the microwave sintered porous Ti-3Cu alloys. J. Alloy. Compd. 812, 152142. https://doi.org/10.1016/j.jallcom.2019.152142.

Yao, H.L., Yang, C., Yang, Q., Hu, X.Z., Zhang, M.X., Bai, X.B., Wang, H.T., Chen, Q.Y., 2020. Structure, mechanical and bioactive properties of nanostructured hydroxyapatite/titania composites prepared by microwave sintering. Mater. Chem. Phys. 241, 122340. https://doi.org/10.1016/j.matchemphys.2019.122340.

Ye, X.L., Guo, S.H., Yang, L., Gao, J.Y., Peng, J.H., Hu, T., Wang, L., Hou, M., Luo, Q.Y., 2018. New utilization approach of microwave thermal energy: Preparation of metallic matrix diamond tool bit by microwave hot-press sintering. J. Alloy. Compd. 748, 645-652. https://doi.org/10.1016/j.jallcom.2018.03.183.

Zhang, T.K., Wu, X.Z., 2004. Speculation of development perspective in Chinese blast furnace ferromanganese. Ferro-Alloys. 35, 43-48. https://doi.org/10.3969/j.issn.1001-1943.2004.06.011.

Zhang, X.B., Han, Y.G., Fang, J.H., Sheng, G., Cheng, H., 2009. Research and practice on enhance the gas yield into the gasometer in wet dust collection of ore heat furnace. Ferro-Alloys. 40, 18-23. https://doi.org/10.3969/j.issn.1001-1943.2009.02.004.

Zhou, L., Huang, J.L., Wang, X.G., Su, G.X., Qiu, J.Y., Dong, Y.L., 2019. Mechanical, dielectric and microwave absorption properties of FeSiAl/Al_2O_3 composites fabricated by hot-pressed sintering. J. Alloy. Compd. 774, 813-819. https://doi.org/10.1016/j.jallcom.2018.09.387.

Table captions

Table 1 Chemical compositions of ferromanganese powder.

Table 2 Thermodynamics data of oxidation reactions of elements in alloy melt.

Table 3 Chemical compositions of the bulk alloy sintered at 1168 °C for 11 min.

Figure captions

Fig. 1 Particle size distribution of ferromanganese powder.

Fig. 2 Process flow chart of preparing bulk alloy by microwave sintering.

Fig. 3 Dependency of ΔG^{θ} on temperatures for oxidation reactions of elements in ferromanganese alloy melt (Thermodynamic data were calculated by thermodynamic software including Fact-sage and HSC 6.0).

Fig. 4 TG-DSC curves of ferromanganese powder (Temperature regime: 20 °C to 1350 °C; heating rate: 30 °C/min; Argon (Ar) flow rate: 60 mL/min).

Fig. 5 Effects of variable factors on volume density properties of the sintered bulk alloy, (a) temperature (Duration time: 10 min; composition proportion: 75%); (b) duration time (Sintering temperature: 1100 °C; composition proportion: 75%); (c) composition proportion of the alloy powder of <75 mm (Sintering temperature: 1100 °C; duration time: 10 min).

Fig. 6 SEM images of (a) ferromanganese powder and (b) the bulk alloy sintered at 1168 °C for 11 min.

Fig. 7 SEM images and EDAX spectra of the bulk alloy sintered at 1168 °C for 11 min, (a) SEM image, 250×; (b) SEM image, 3000×; (e) EDAX spectra.

Table 1 Chemical compositions of ferromanganese powder.

Compositions	Mn	Fe	C	Si	P	S
Mass/W%	76.47	15.53	6.40	1.41	0.17	0.02

Table 2 Thermodynamics data of oxidation reactions of elements in ferromanganese alloy melt.

Reactions	ΔH^{θ}/ J.mol^{-1}	ΔS^{θ}/ J.(mol.K)$^{-1}$
$2Mn(l) + O_2(g) = 2MnO(s)$	-812698	-177.57
$2Fe(l) + O_2(g) = 2FeO(s)$	-476139	-89.91
$2C(S) + O_2(g) = 2CO(g)$	-235978	168.70
$Si(l) + O_2(g) = SiO_2(l)$	-936379	-168.70
$2/3Mn(l) + 2/3Si(l) + O_2(g) = 2/3MnSiO_3(l)$	-925283	-200.54

Table 3 Chemical compositions of the bulk alloy sintered at 1168 °C for 11 min.

Elements	Mn	Fe	C	Si	P	S
Mass/W%	76.11	15.91	6.21	1.63	0.12	0.02

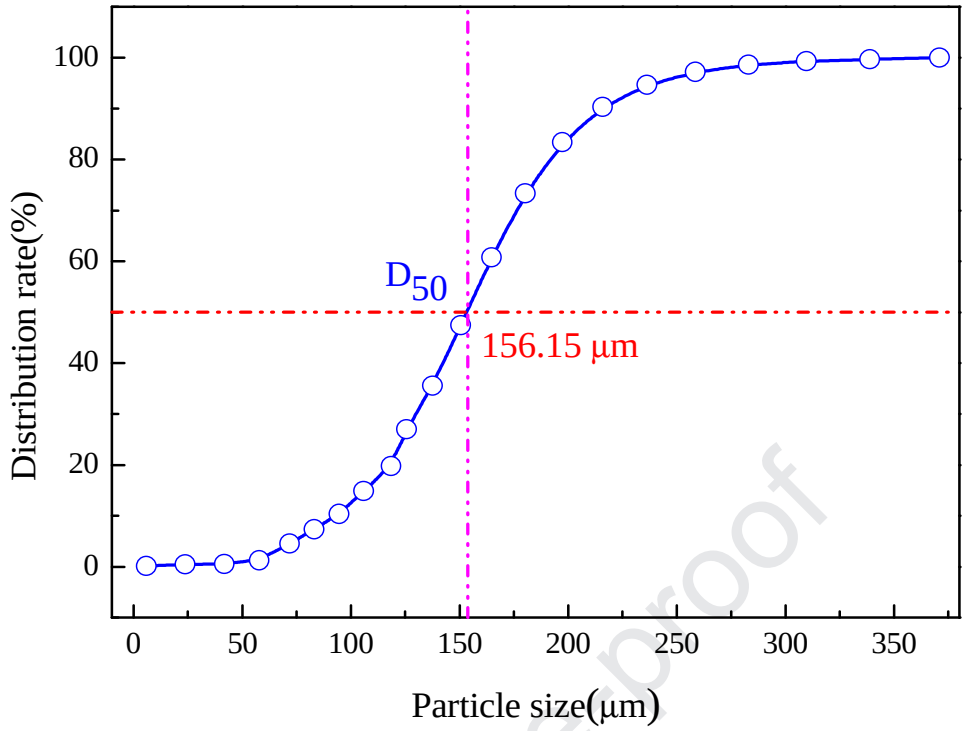

Fig. 1 Particle size distribution of ferromanganese powder.

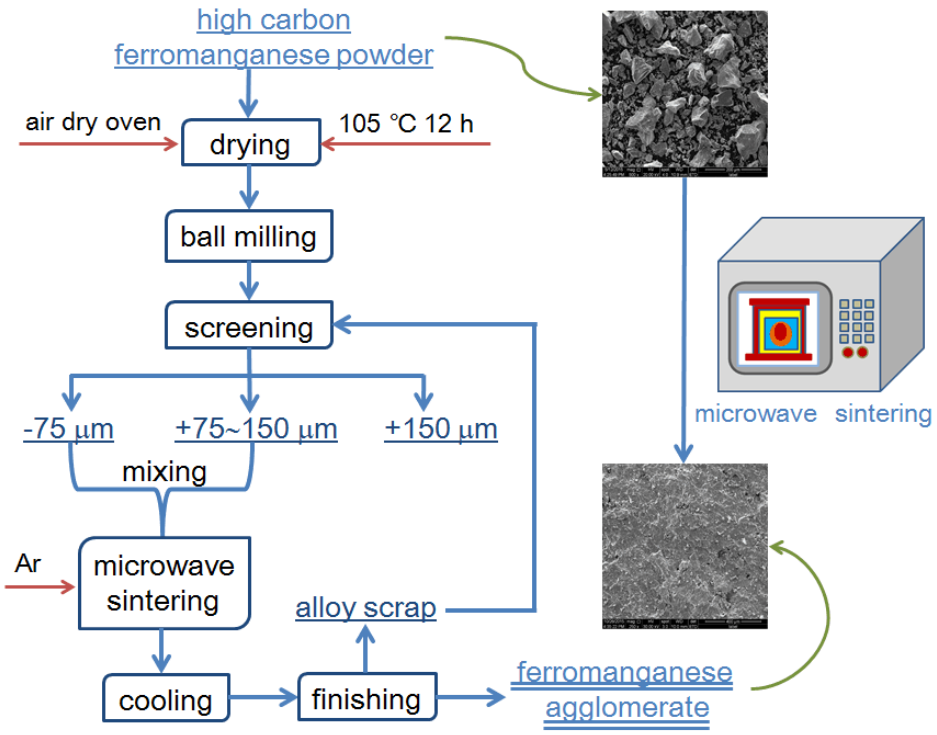

Fig. 2 Process flow chart of preparing bulk alloy by microwave sintering.

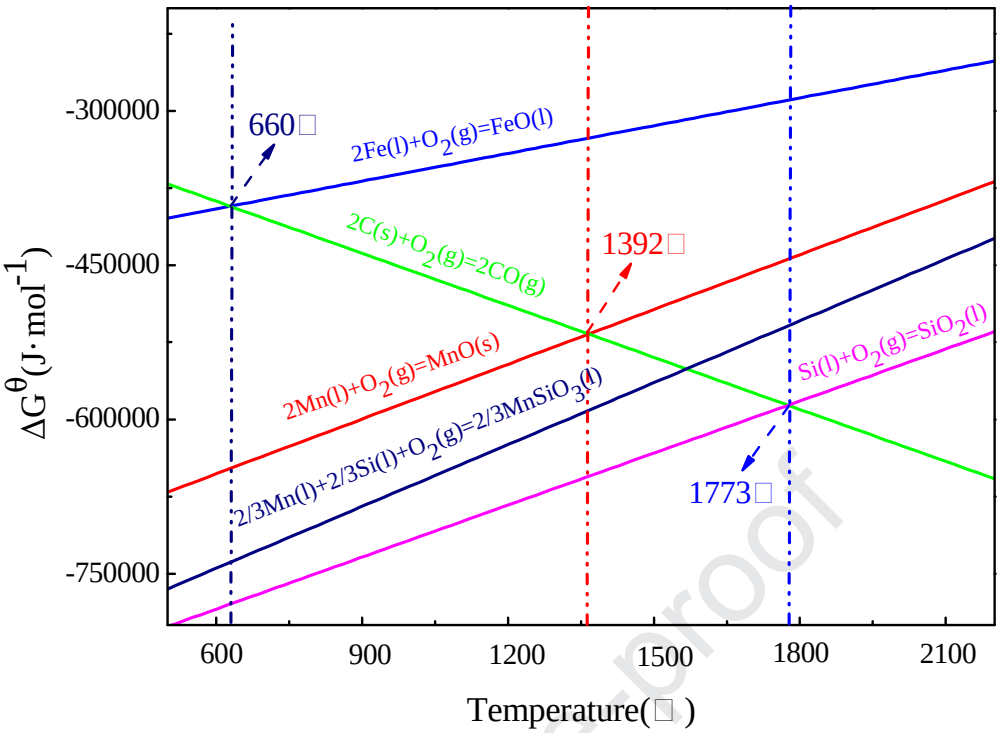

Fig. 3 Dependency of ΔG^{θ} on temperatures for oxidation reactions of elements in ferromanganese alloy melt (Thermodynamic data were calculated by thermodynamic software including Fact-sage and HSC 6.0).

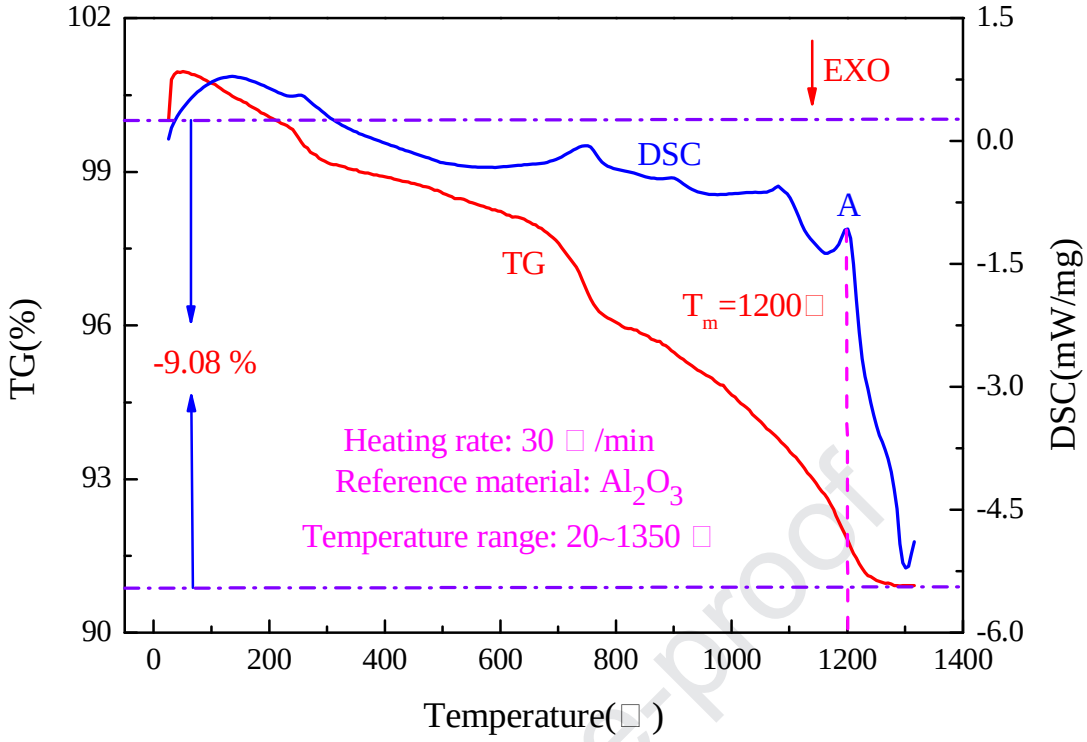

Fig. 4 TG-DSC curves of ferromanganese powder (Temperature regime: 20 °C to 1350 °C; heating rate: 30 °C/min; Argon (Ar) flow rate: 60 mL/min).

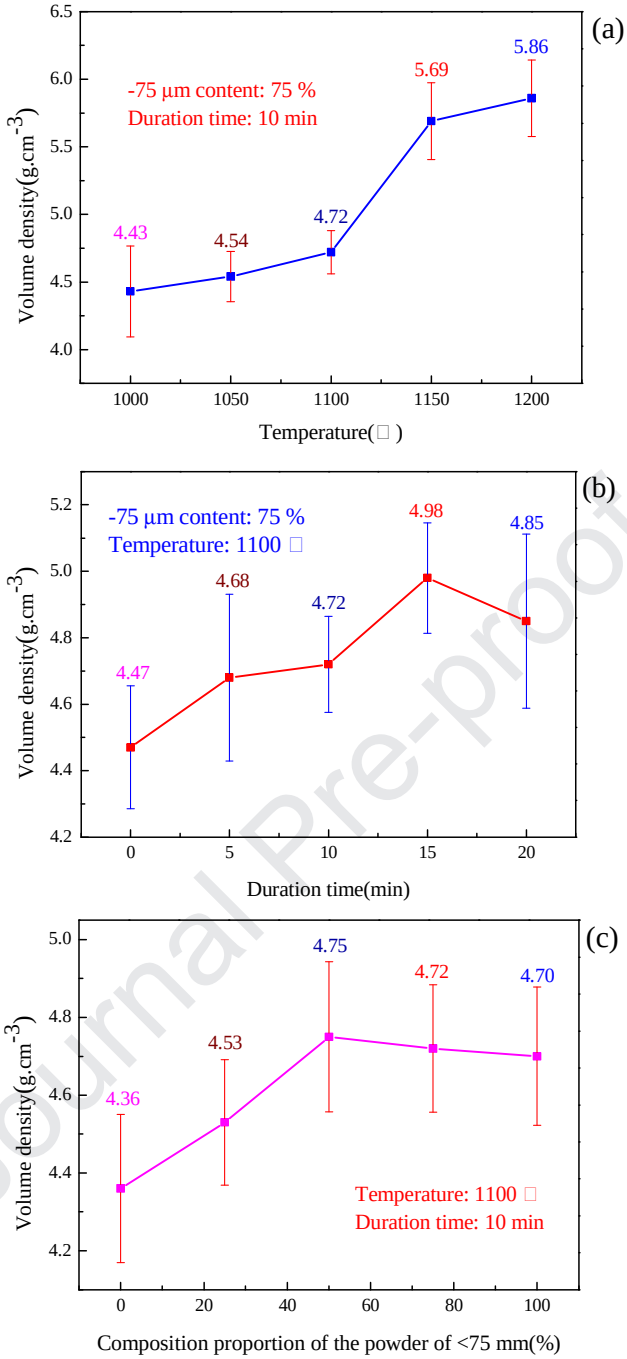

Fig. 5 Effects of variable factors on volume density properties of the sintered bulk alloy, (a) temperature (Duration time: 10 min; composition proportion: 75%); (b) duration time (Sintering temperature: 1100 °C; composition proportion: 75%); (c) composition proportion of the alloy powder of <75 mm (Sintering temperature: 1100 °C; duration time: 10 min).

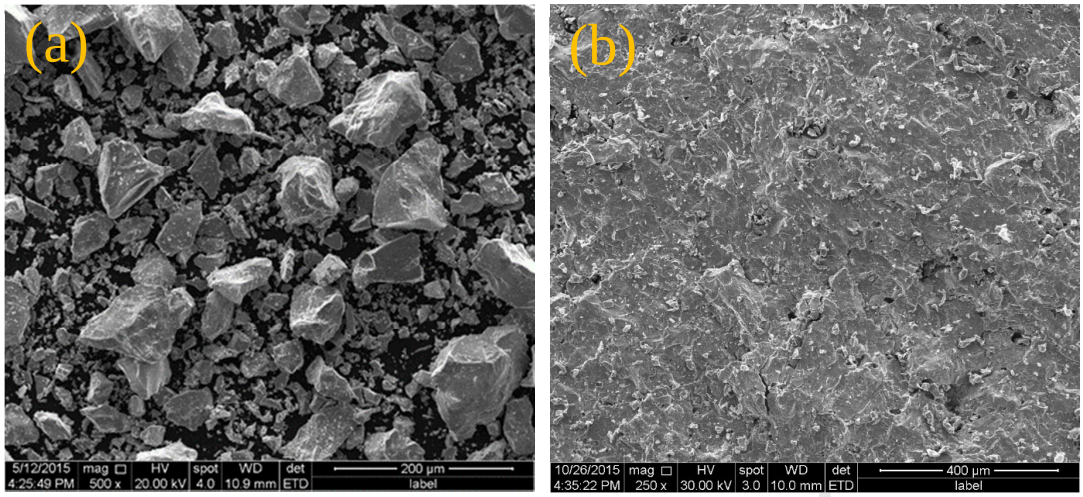

Fig. 6 SEM images of (a) ferromanganese powder and (b) the bulk alloy sintered at 1168 °C for 11 min.

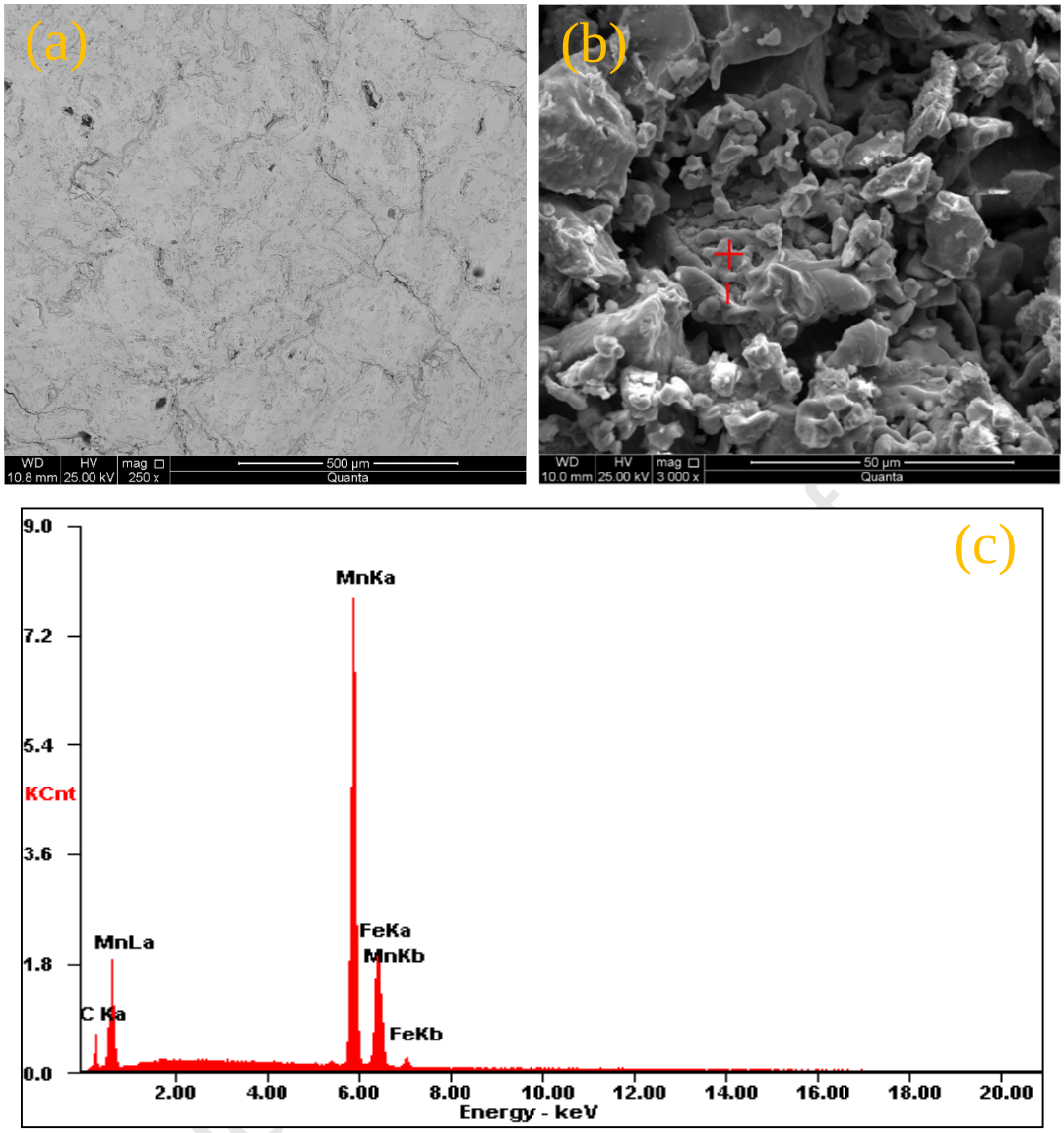

Fig. 7 SEM images and EDAX spectra of the bulk alloy sintered at 1168 °C for 11 min, (a) SEM image, 250×; (b) SEM image, 3000×; (e) EDAX spectra.

Declaration of interests

☒ The authors declare that they have no known competing financial interests or personal relationships that could have appeared to influence the work reported in this paper.

☐The authors declare the following financial interests/personal relationships which may be considered as potential competing interests: